

Lucas Vinicius Rezende Sanches¹, Gustavo Luiz Olichevis Halila², Felipe Issamu Kitadani Odaguil² & João Luiz F. Azevedo³

¹Universidade Federal do Paraná, 81530-900 Curitiba, PR, Brazil.
 ²Embraer, 12227-901 São José dos Campos, SP, Brazil.
 ³Instituto de Aeronáutica e Espaço, 12228-904 São José dos Campos, SP, Brazil.

Abstract

Transonic wing design involves challenges related to the complex physical phenomena associated with this flow regime. Shock waves are present in the flow, rendering it highly nonlinear. Turbulent boundary layers tend to present complex topologies in transonic flow, and their interaction with the shock wave may originate shock-buffet instabilities. Therefore, Computational Fluid Dynamics (CFD) approaches are required in the preliminary design phase. A rigorous exploration of the design space must be performed to originate aero-dynamically efficient configurations. Gradient-based shape optimization is the choice to perform aerodynamic shape optimization (ASO) of transonic wings. The adjoint method is the most efficient way to compute the required derivatives within the desired accuracy levels. In this paper, we investigate the effects of the number of free form deformation (FFD) control points over the optimized wing drag coefficient and configuration topology. Our results indicate that increasingly refined FFD grids lead to additional drag coefficient reductions while respecting geometric and lift coefficient constraints.

Keywords: Transonic Wing Design, Aerodynamic Shape Optimization, Adjoint Method

1. Introduction

The transonic flow domain is affected by complex phenomena such as shock waves, drag divergence, and transonic buffet [1]. One relevant aspect of transonic flow is the importance of nonlinear aerodynamic effects. Bendiksen [2] points out that transonic flow over aircraft wings is nonlinear even in the limit of small disturbances. In addition to the aspects highlighted above, advanced aircraft aerodynamics involves complex physical phenomena, such as transition to turbulence, flow separation, and wake interaction, among others. Computational tools that are able to consider these phenomena are fundamental to the design of efficient aircraft. These aspects indicate the need to perform Reynolds-averaged Navier–Stokes (RANS) simulations as soon as during the preliminary design phase. A rigorous design space exploration is required to engineer efficient airframes. When RANS simulations are considered in the optimization loop, gradient-based optimization is a requirement due to its computational efficiency.

Aerodynamic shape optimization (ASO) is an effective tool to better explore the aerodynamics design space. Optimization algorithms can be based on gradients and Hessians, in the so called gradient-based optimization class, or use approaches that do not use this mathematical information, in the class of gradient-free optimization algorithms. A comparison between genetic and gradient-based optimization algorithms applied to ASO can be found in Ref. [3]. For ASO problems, which usually involve a large number of design variables, gradient-based algorithms are the only viable alternative as

the number of function evaluations and overall cost are smaller than in the gradient-free case [4, 5]. Considering the industry requirements that make a high volume of configuration evaluations mandatory, the use of gradient-based ASO is necessary. To compute the derivatives in an inexpensive way, adjoint methods are used. In the adjoint method, the cost scales with the number of design objectives rather than with the number of design variables [6], which makes it ideal for use in ASO studies.

Adjoint methods were first used within the optimal controls community, with the work of Lions [7] and Bryson and Ho [8]. Adjoint methods were then used to solve structural optimization problems [9, 10]. The use of the adjoint method in fluid mechanics was first introduced by Pironneau [11], who derived the adjoints of the Stokes equations and of the Euler equations [12]. In 1988, Jameson [13] extended the method to inviscid compressible flows, making it suitable for transonic airfoil design. The adjoint method was then applied to the Navier–Stokes equations by Jameson et al. [14] and by Nielsen and Anderson [15].

At present, complex aircraft configurations are optimized considering high-fidelity, RANS-based CFD calculations. A multipoint optimization approach encompassing a broad range of operating conditions in the objective function and constraints was used to perform aerodynamic shape optimization in Ref. [16]. Planar and nonplanar wings were optimized in Ref. [17], while both multimodality and global optimizations were discussed in Ref. [18]. The optimization of regional aircraft configurations was performed in Ref. [19]. Lyu et al. [20] were able to perform a lift-constrained drag minimization of the NASA Common Research Model (CRM) wing with a RANS turbulence model. The corresponding wing-body-tail configuration was also optimized [21]. An aerostructural optimization has also been performed by Kenway and Martins [22], and a boundary layer ingestion propulsion system was investigated using adjoint-based ASO [23]. Laminar flow design assisted by adjoint-based ASO were performed in Refs. [24, 25, 26, 27, 28]. Discussions in Ref. [29] addressed the use of an adjoint method approach to control unsteady flows.

In this paper, we perform high-fidelity, adjoint-based ASO for transonic wings. In special, we focus on the impact of the number of design variables over the optimal design. We use free form deformation (FFD) to parametrize the configuration and employ FFD grids with different numbers of control points in both chordwise and spanwise directions. Our results indicate that increasingly refined FFD grids lead to additional drag coefficient reductions while respecting geometric and lift coefficient constraints. All of our single-point aerodynamic shape optimizations lead to shock-free transonic flow at the operating point.

This paper is organized as follows. Our flow solver and the SA turbulence model formulation are described in Sec. 2. A review of the discrete adjoint method is presented in Sec. 3. Numerical results are provided in Sec. 4. We end the paper with final remarks in Sec. 5.

2. Flow Solver and Turbulence Modeling

2.1 CFD Solver

We use ADflow to perform the simulations whose results are included in this paper. ADflow is an open source, in-house CFD solver, which was developed and is maintained at the University of Michigan. ADflow has options to solve Euler, laminar Navier—Stokes, and RANS equations in steady, unsteady, and time-spectral modes, with multiblock structured and overset meshes. The governing equations are discretized using the finite volume method with first and second order stencils. A pseudo-transient continuation (PTC) strategy is used to converge the flow equations. The inviscid fluxes are discretized by using three different numerical schemes: the scalar Jameson—Schmidt—Turkel [30] (JST) artificial dissipation scheme, a matrix dissipation scheme based on the work of Turkel and Vatsa [31], and a monotone upstream-centered scheme for conservation laws (MUSCL) based on the work of van Leer [32] and Roe [33]. The viscous flux gradients are calculated by using the Green—Gauss approach. The residual equations can be converged with four distinct algorithms. Runge-Kutta and diagonalized-diagonally-dominant alternating direction implicit [34] (D3ADI) algorithms are available. An approximate Newton—Krylov [35] (ANK) solver is also implemented and can be used as a glob-

alization scheme for the full Newton-Krylov algorithm [36]. Due to its robustness and numerical behavior, we adopt the ANK solver in this work. Further details on ADflow can be found in Ref. [37].

Our aerodynamic shape optimization (ASO) framework uses ADflow as the flow solver. The adjoint flow solvers are also integrated in ADflow. The design variable vector, \mathbf{x} , contains both aerodynamic and geometric design variables. While derivatives of the objective function with respect to aerodynamic design variables are computed directly, we use a chain rule to calculate derivatives with respect to geometric design variables. This is,

$$\frac{d\mathbf{f}}{d\mathbf{x}} = \frac{d\mathbf{f}}{d\mathbf{x}_{\mathsf{V}}} \frac{d\mathbf{x}_{\mathsf{V}}}{d\mathbf{x}_{\mathsf{S}}} \frac{d\mathbf{x}_{\mathsf{S}}}{d\mathbf{x}},\tag{1}$$

where subscripts v and s indicate, respectively, the volume and the design surface coordinates. We compute the derivatives $d\mathbf{x}_{\rm S}/d\mathbf{x}$ and $d\mathbf{x}_{\rm V}/d\mathbf{x}_{\rm S}$ by using two external open-source geometry modules, pyGeo [38] and IDWarp [39]. In pyGeo, the geometry is parametrized using the free-form deformation (FFD) technique. The FFD is a mapping of a region in 2-D or 3-D that is bounded by a set of B-splines. The B-splines are defined by a set of control points that constitute the shape design variables. As we perform constrained optimization, we also compute the geometric constraint derivatives. More details on the FFD technique can be found in Ref. [40]. In IDwarp, an efficient analytic inverse-distance method [41] is used. The derivative $d\mathbf{f}/d\mathbf{x}_{\rm V}$ is computed in ADflow. By doing this, we assure that the adjoint implementation does not depend on external geometric parametrization and mesh deformation modules [42, 43].

2.2 Spalart-Allmaras Turbulence Model

The Spalart–Allmaras turbulence model [44] is selected for all numerical results presented in this paper. Results in Ref. [45] indicate that the SA model performs better for buffet computations than the Shear Stress Transport [46] (SST) turbulence model. In the study described in Ref. [45], the authors point out that the SST model failed to predict stable buffet when used without a wall law strategy. The governing equation for the SA model working variable, \tilde{v} , reads,

$$\frac{D\tilde{\mathbf{v}}}{Dt} = c_{b1}S\tilde{\mathbf{v}}\left(1 - f_{t2}\right) - \left(c_{w1}f_{w} - \frac{c_{b1}}{\kappa^{2}}f_{t2}\right)\left(\frac{\tilde{\mathbf{v}}}{d}\right)^{2} + \frac{1}{\sigma}\left\{\frac{\partial}{\partial x_{i}}\left[\left(\mathbf{v} + \tilde{\mathbf{v}}\right)\frac{\partial\tilde{\mathbf{v}}}{\partial x_{i}}\right] + c_{b2}\frac{\partial\tilde{\mathbf{v}}}{\partial x_{i}}\frac{\partial\tilde{\mathbf{v}}}{\partial x_{i}}\right\}.$$
(2)

The relation between the SA working variable, \tilde{v} , and the eddy viscosity, μ_t , can be written as,

$$\mu_t = \rho \tilde{v} \frac{\chi^3}{\chi^3 + c_{vl}^3},\tag{3}$$

where

$$\chi = \frac{\tilde{v}}{v}.\tag{4}$$

Allmaras and Johnson [47] describe the other variables in Eqs. (2) to (4) in more detail.

3. The Adjoint Method

The adjoint method provides an inexpensive way to compute derivatives [48]. In aerodynamic shape optimization it is usual that a large number of design variables is used, making the adjoint method specially useful. When using the adjoint method to compute derivatives, two main approaches are available. If one differentiates the governing equations prior to discretization, the method is referred to as continuous adjoint. If the equations are discretized first and the resulting system is used to write the corresponding adjoint equation, the discrete approach is used.

The continuous approach generates a linearized partial differential equation (PDE) that can, in general, be solved with the same numerical method used to address the primal problem, eliminating

the need to explicitly assemble the Jacobian and leading to a memory-efficient adjoint code [6]. On the negative side, the continuous adjoint implementations present low accuracy on coarse meshes. Since the PDEs are first linearized and, then, discretized in the continuous approach, the discretized form of these linearized equations will only yield a fully consistent gradient in the limit of an infinitely fine mesh [49]. The boundary conditions to be used with the linearized PDEs are also not straightforward. Finally, the need to perform manual differentiation of the PDEs presents an additional challenge that has led to implementations where some terms of the turbulence model are simplified, creating an additional source of error [50].

In the discrete approach, the exact gradient of the discrete objective function is achieved independently of the coarsness of the mesh [51, 50, 6]. In this approach, the partial derivatives involved in the adjoint calculation can be easily obtained using algorithmic differentiation [52]. When using the discrete adjoint approach, an efficient implementation is important since the computational and memory costs associated with this approach are high. In this work, we adopt the discrete adjoint approach. Further comparisons between the discrete and continuous approaches are available in the literature [51, 49].

In a general optimization problem, our objective function, $\mathbf{f} = \mathbf{F}(\mathbf{x}, \mathbf{y}(\mathbf{x}))$, is a vector of size n_f . The governing equations are associated with the n_y states composing the $\mathbf{y}(\mathbf{x})$ vector, sized n_x . The idea behind the adjoint method is that the sensitivities of a given objective function \mathbf{f} to a given perturbation in the design variables $(\mathbf{x} + \delta \mathbf{x})$ can be computed without solving the complete primal problem for the perturbed design variable conditions.

The governing equations can be written under the form of residuals,

$$\mathbf{r} = \mathbf{R}(\mathbf{x}, \mathbf{y}(\mathbf{x})) = \mathbf{0}. \tag{5}$$

The total derivative of the objective function **f** with respect to the design variables can be expressed as,

$$\frac{d\mathbf{f}}{d\mathbf{x}} = \frac{\partial \mathbf{F}}{\partial \mathbf{x}} + \frac{\partial \mathbf{F}}{\partial \mathbf{y}} \frac{d\mathbf{y}}{d\mathbf{x}},\tag{6}$$

where the resulting Jacobian is an $(n_f \times n_x)$ matrix. Partial derivatives represent the variation of $\mathbf{f} = \mathbf{F}(\mathbf{x})$ for a fixed state vector \mathbf{y} meaning that, here, the residuals are different from zero because the design variables are perturbed but the states, \mathbf{y} , are not updated accordingly. This represents an explicit relation of the objective function vector with the design variables. On the other hand, the total derivatives such as $d\mathbf{f}/d\mathbf{x}$ and $d\mathbf{y}/d\mathbf{x}$, take into account the change in the states \mathbf{y} that are required to keep the residual equations equal to zero, which corresponds to an implicit relation. When adjoint methods are used, re-solving the primal system to obtain the corresponding updated states $(\mathbf{y} + \delta \mathbf{y})$ such that $\mathbf{R}(\mathbf{x} + \delta \mathbf{x}, \mathbf{y} + \delta \mathbf{y}) = \mathbf{0}$ is not required to obtain the desired sensitivity of the objective function with respect to the design variable perturbation, $d\mathbf{f}/d\mathbf{x}$. Partial derivatives can be computed using finite differences, complex step, or algorithmic differentiation.

Because the governing equations must always be satisfied, the total derivative of the residuals, Eq. (5), with respect to the design variables, must also be zero,

$$\frac{d\mathbf{r}}{d\mathbf{x}} = \frac{\partial \mathbf{R}}{\partial \mathbf{x}} + \frac{\partial \mathbf{R}}{\partial \mathbf{y}} \frac{d\mathbf{y}}{d\mathbf{x}} = \mathbf{0}.$$
 (7)

The computation of the total derivative $d\mathbf{y}/d\mathbf{x}$ in Eqs. (6) and (7) represents a high computational cost because the residual equations must be solved for the perturbed design variables. On the other hand, the partial derivatives present in these equations can be computed in an inexpensive manner because \mathbf{y} is kept constant for the perturbed design variables since the residual equations are not solved.

By rewriting the linearization in Eq. (7) as

$$\frac{\partial \mathbf{R}}{\partial \mathbf{y}} \frac{d\mathbf{y}}{d\mathbf{x}} = -\frac{\partial \mathbf{R}}{\partial \mathbf{x}},\tag{8}$$

we can write Eq. (6) as

$$\frac{d\mathbf{f}}{d\mathbf{x}} = \frac{\partial \mathbf{F}}{\partial \mathbf{x}} - \frac{\partial \mathbf{F}}{\partial \mathbf{y}} \left(\frac{\partial \mathbf{R}}{\partial \mathbf{y}} \right)^{-1} \frac{\partial \mathbf{R}}{\partial \mathbf{x}}.$$
 (9)

If small design variable perturbations are assumed, the adjoint (Ψ) equation reads

$$\left(\frac{\partial \mathbf{R}}{\partial \mathbf{y}}\right)^{T} \Psi + \left(\frac{\partial \mathbf{F}}{\partial \mathbf{y}}\right)^{T} = \mathbf{0},\tag{10}$$

where Ψ is the adjoint matrix of size $(n_y \times n_f)$, its n^{th} component is the sensitivity of **f** to changes in the n^{th} residual. By combining Eqs. (9) and (10), we obtain,

$$\frac{d\mathbf{f}}{d\mathbf{x}} = \Psi^T \frac{\partial \mathbf{R}}{\partial \mathbf{x}} + \frac{\partial \mathbf{F}}{\partial \mathbf{x}}.$$
 (11)

To solve Eq. (11) for the desired sensitivity, $d\mathbf{f}/d\mathbf{x}$, we need the solution for the adjoint field, Ψ , from Eq. (10). The linear system expressed in Eq.(10) must be solved for each column of $(\partial \mathbf{F}/\partial \mathbf{y})^T$ and, therefore, its computational cost scales with the number of quantities of interest, n_f , and is independent of the number of design variables, n_x . Hence the adjoint method is effective for cases where the number of design variables, n_x , exceeds the number of quantities of interest, n_f . This is often the case in aerodynamic shape optimization, where there might be hundreds of shape design variables, but only a few quantities of interest, such as drag, aerodynamic efficiency, or other equivalent metrics.

4. Numerical Results

In this section, we present the results for the adjoint-based aerodynamic shape optimization (ASO) for a transonic wing. We use FFD grids with varying numbers of control points in both chordwise and spanwise directions, and investigate the impact of the number of shape design variables over the final design. For all of our numerical optimizations, we use the Sequential Least Squares Quadratic Programming (SLSQP) optimizer [53], which is particularly suitable for solving nonlinear optimization problems. The SLSQP algorithm approximates the original problem with a sequence of quadratic problems (QP) [54].

Our numerical results consider a baseline configuration that represents a transonic wing based on the RAE 2822 airfoil. This baseline configuration is part of the University of Michigan MDO Lab documentation [55]. The baseline wing configuration is depicted in Fig. 1. Our computational mesh, which is shown in Fig. 2, has 2,644,922 cells and an off-wall spacing resulting in y^+ values no larger than 1.

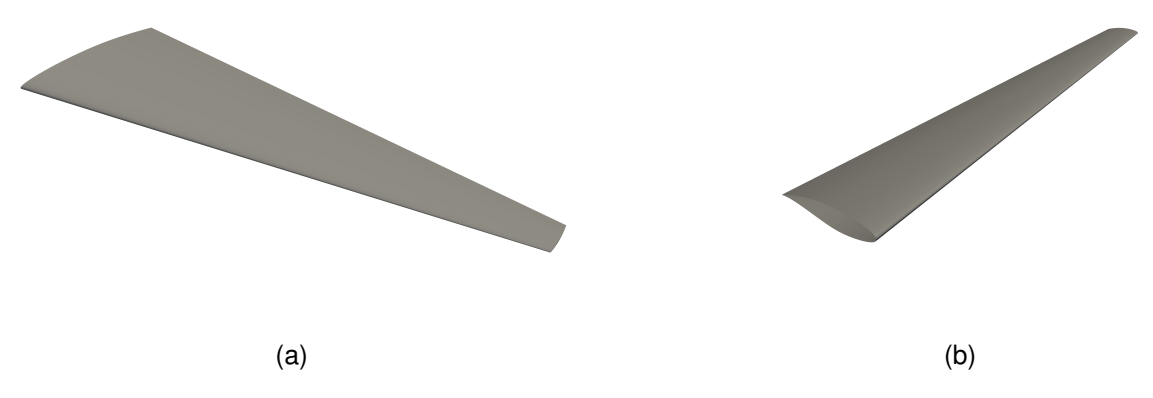


Figure 1 – Baseline wing configuration.

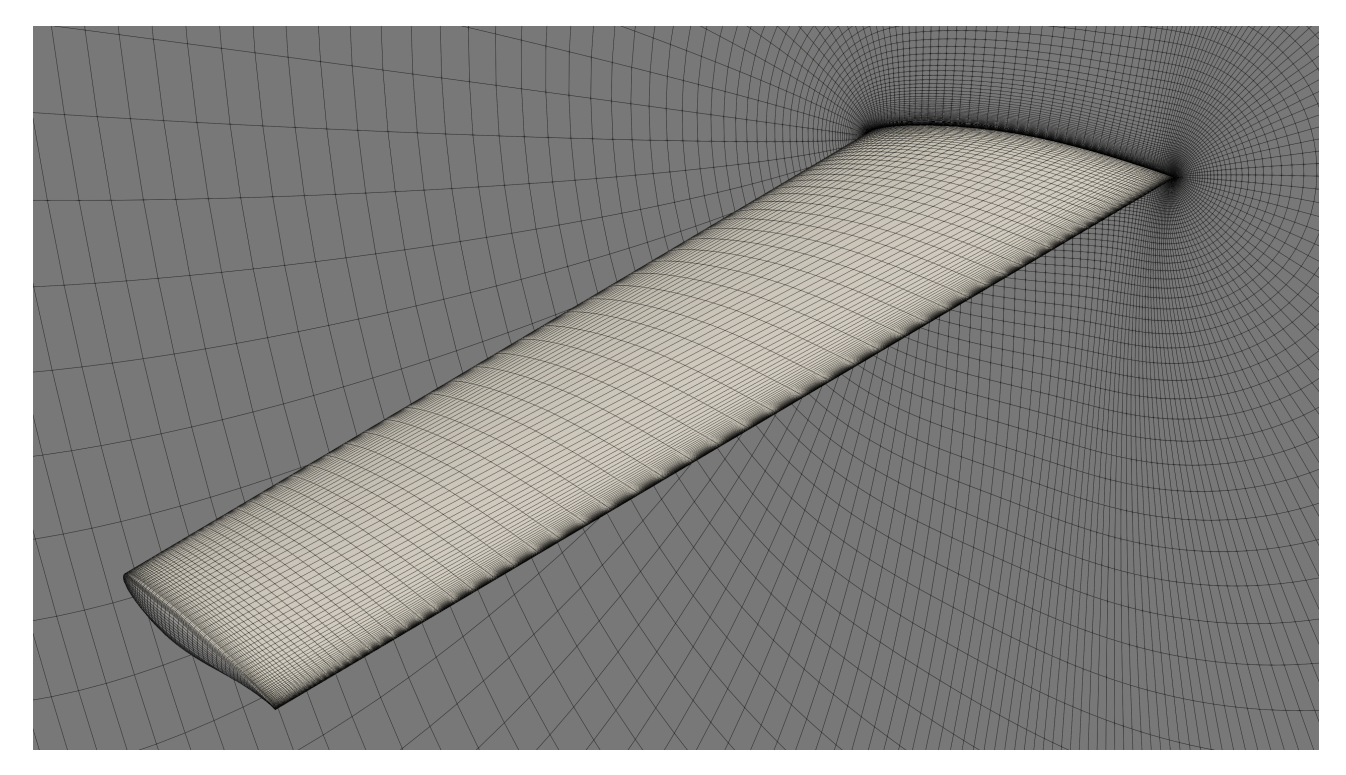


Figure 2 – Computational mesh with 2,644,922 cells used during the optimizations presented here.

Relevant planform information related to the baseline wing are shown in Table 1. We consider a freestream Mach number of 0.8 and a mean aerodynamic chord-based Reynolds number of 4.58×10^7 . For all of the optimizations presented here, we start from an angle of attack of 1.5 degree.

We focus on drag minimization and target a lift coefficient of $C_L = 0.45$, performing single-point aerodynamic shape optimizations at the operating Reynolds and Mach numbers. Our design variables are the FFD control points, which control the sectional shapes, twist global design variables, and the angle of attack. The twist design variables act such as each of the spanwise FFD sections rotate around an axis that passes through the quarter chord. The FFD section placed at the wing root is not included as a twist design variable, so that the wing root will not twist. We impose thickness and internal volume constraints and ask the baseline values for these quantities to be equaled or superseded by the optimum design. In order to prevent the local shape variables from creating a shearing twist, which can arise when using both twist and local shape variables, we constrain the upper and lower FFD control points on the leading (LE) and trailing (TE) edges to move in opposite directions. These constraints are imposed at each of the spanwise FFD sections. Our general optimization problem is summarized in Table 2.

Table 1 – Baseline wing planform data

Root chord [m]	Tip chord [m]	Semi-span [m]	Sweep angle at quarter chord [degrees]
5	1.5	14	7.5

We use FFD grids with varying numbers of control points. The control points are linearly spaced in both spanwise and chordwise directions. In the FFD designations, the first digit represents the number of control points in the chordwise direction, while the second one indicates the number of FFD degrees of freedom in the spanwise direction. For instance, the FFD 8-16 represents a box with 8 points in each of the section sides, or 16 points per section. Considering the 16 points in the spanwise direction, the FFD 8-16 encapsulates a total of 256 points. An image of the FFD 8-16 grid is presented in Fig. 3. As noted in Table 2, the leading and trailing control points move in opposite direction as to avoid twisted geometries.

Table 2 – Aerodynamic shape optimization problem

	Function/variable	Description	Quantity
minimize	C_D	Drag coefficient	1
with respect to	lpha z au	Angle of attack FFD control point z-coordinates Twist of each FFD section	1 Variable Variable
subject to	$C_L = 0.45$ $t \geq t_{ exttt{base}}$ $V \geq V_{ exttt{base}}$ $\Delta z_{ exttt{TE;upper}} = -\Delta z_{ exttt{TE;lower}}$	Lift coefficient constraint Thickness constraint Volume constraint Constraints to prevent TE shearing twist	1 100 1 Variable
	$\Delta z_{LE;upper} = -\Delta z_{LE;lower}$	Constraints to prevent LE shearing twist	Variable

For a lift coefficient of 0.45, which is the desired target for all the optimizations presented here, the baseline wing presents a drag coefficient of 181.6 drag counts. Results for ASO simulations considering multiple FFD configurations are presented in Table 3. The coarser FFD grid, reference 4-12, results in a drag coefficient of 153.4 drag counts. This represents a 15.53% drag reduction with respect to the baseline geometry. When the FFD discretization is increased in the chordwise direction and reduced in the spanwise direction, resulting in FFD 6-8, the drag coefficient is further reduced to 153.2 drag counts. A further increase in the number of spanwise control points, leading to FFD 6-14, results in a drag coefficient of 152.3 drag counts, while FFD 6-16 yields a drag coefficient of 151.6 drag counts. When the chordwise FFD discretization is increased to 8 points, combined with 12 spanwise control points, FFD 8-12, the drag coefficient rises to 152.7 drag counts. Comparing this result with the ones corresponding to FFDs 6-14 and 6-16 leads to the impression that, for the FFD configurations presented here, the spanwise discretization has a more pronounced impact on the drag coefficient than the chordwise resolution. The finest FFD grid, 8-16, leads to a drag coefficient of 151.4 drag counts, which corresponds to a 16.63% drag coefficient reduction with respect to the baseline wing at the same lift coefficient.

Table 3 – Drag coefficient for optimized wing corresponding to multiple FFD configurations

Control points (FFD)	Optimized C_D (10 ⁴)	Drag difference (%)
4-12	153.4	15.53
6-8	153.2	15.64
6-14	152.3	16.13
6-16	151.6	16.52
8-12	152.7	15.91
8-16	151.4	16.63

Figure 5 provides pressure coefficient, C_p , contours for the optimized designs corresponding to each of the FFD configurations. Baseline and optimized wing sections, with corresponding C_p distributions, are also displayed. In Fig. 5, blue lines indicate baseline wing sections, while red ones represent optimized geometries. Normalized lift, twist, and thickness distributions are also shown in Fig. 5. One can see that, for all of the optimized configurations, the optimizer leads to shock-free flows. This can be observed in both wing pressure coefficient contours and sectional C_p distributions. The optimizer also delivers configurations with outer section wash-out, which is typical of transonic wing design. The inner wing sections are adjusted as to provide the wing with wash-in twist, which is also beneficial in transonic wing design. Possible lack of mesh resolution and difficulties naturally associated with

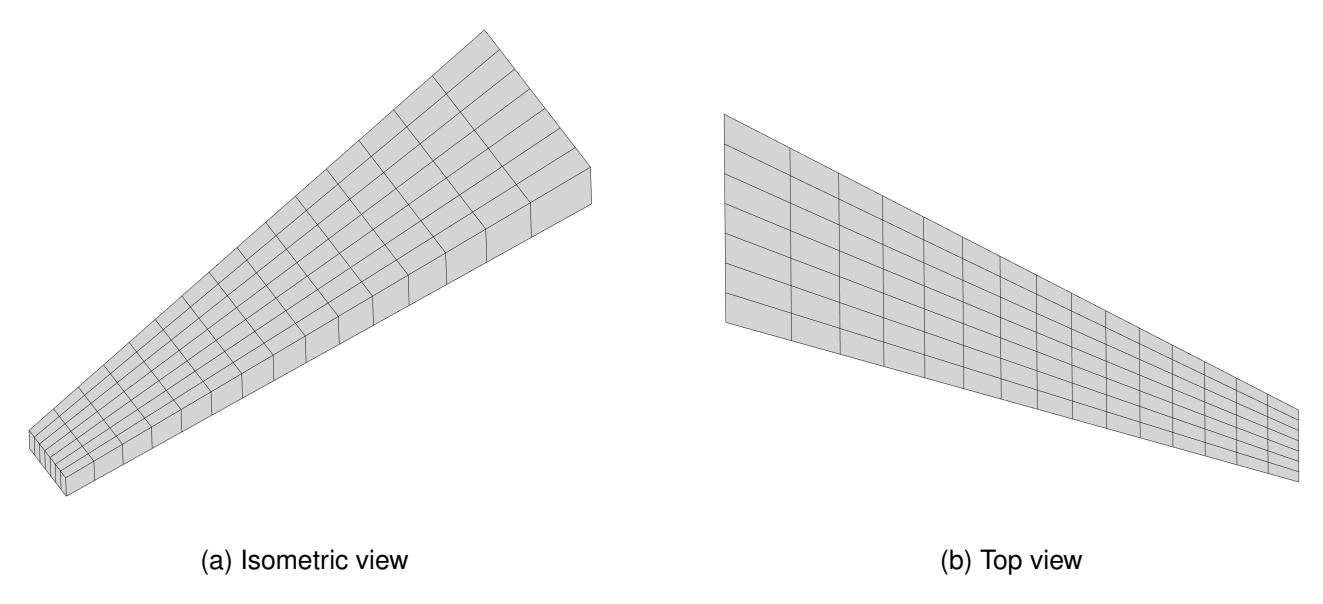
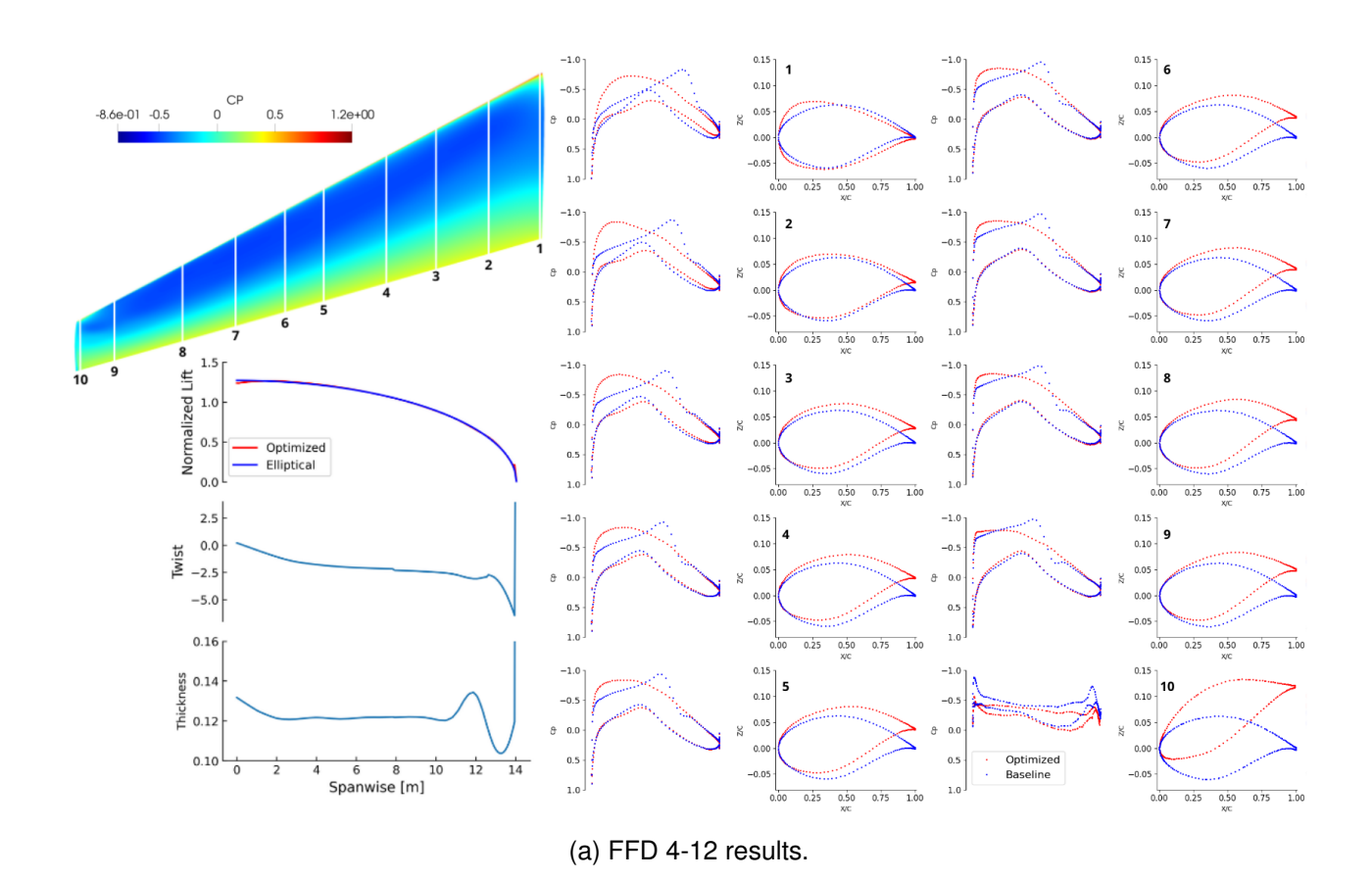
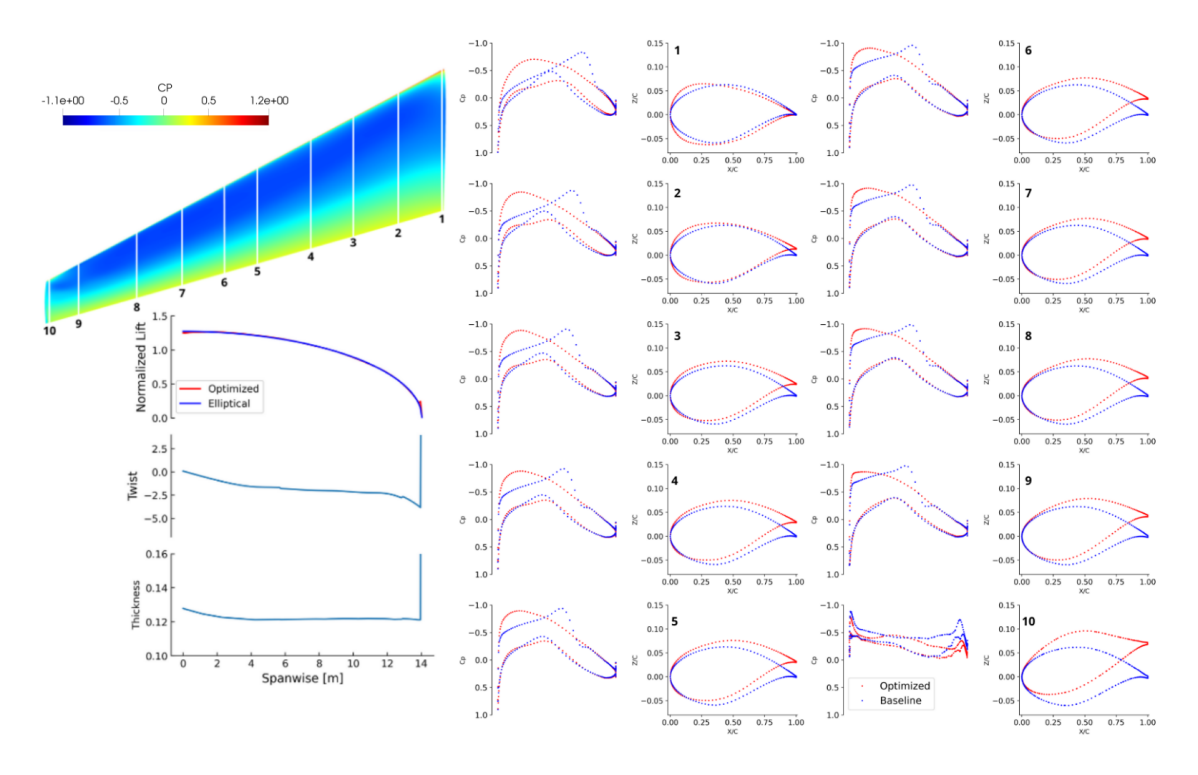


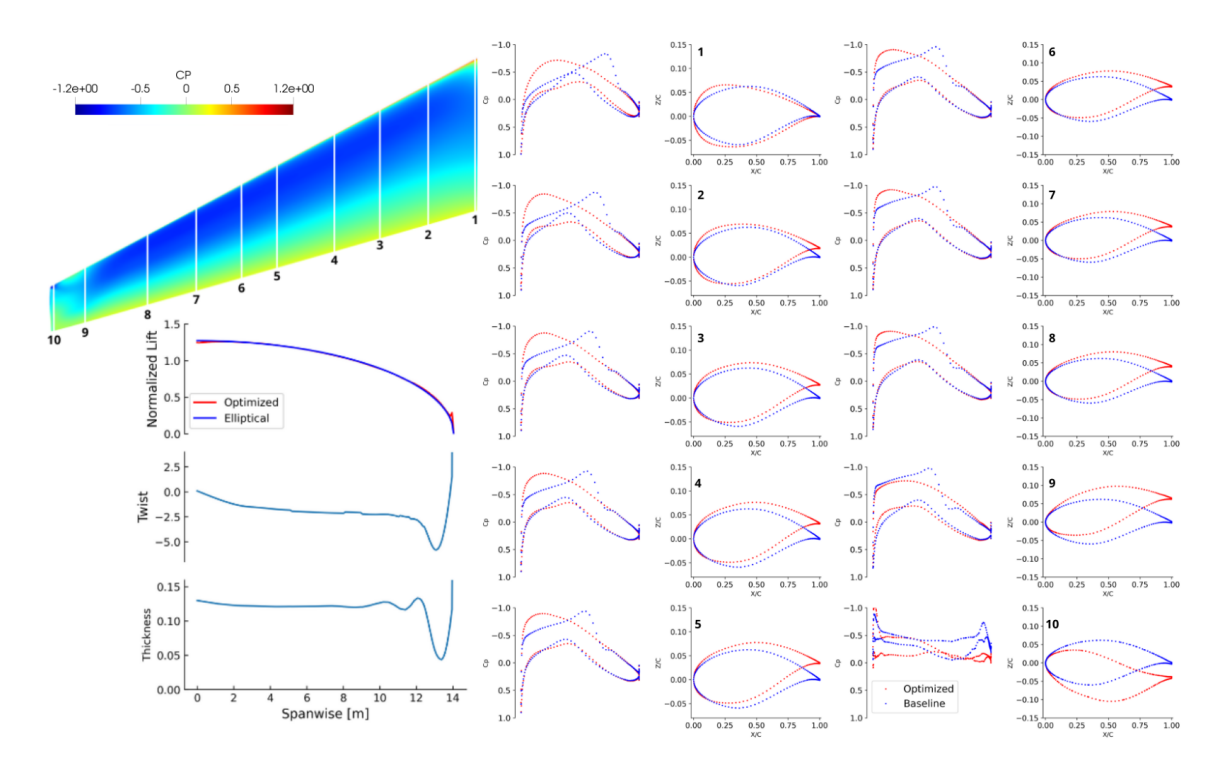
Figure 3 – Free form deformation grid with 256 control points.

the wingtip vortical flow solution result in twisted shapes in the outermost wing sections for FFDs 6-14, 6-16, 8-12, and 8-16. Optimized shapes corresponding to FFDs 6-14, 6-16, 8-12, and 8-16 present waviness in the outer wing sections, which can be inferred from their corresponding thickness distributions. This could be avoid by imposing more stringent geometric constraints or using additional FFD architectures.

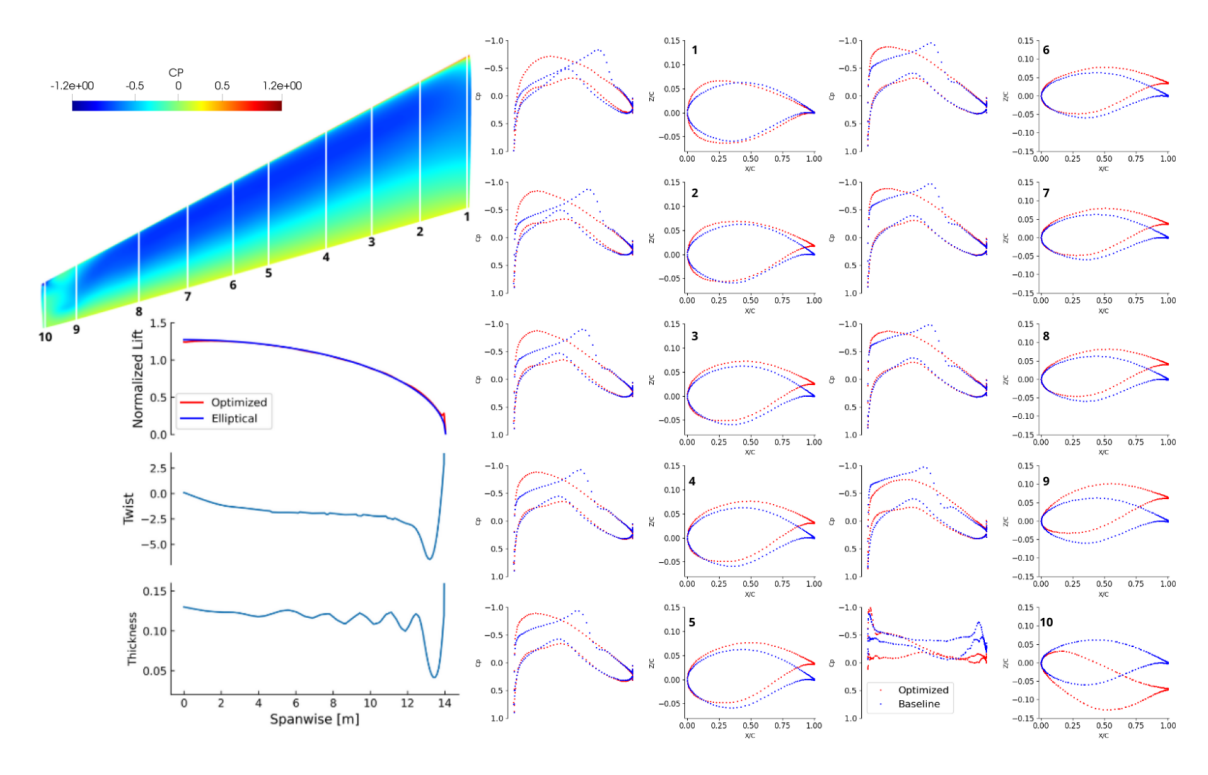




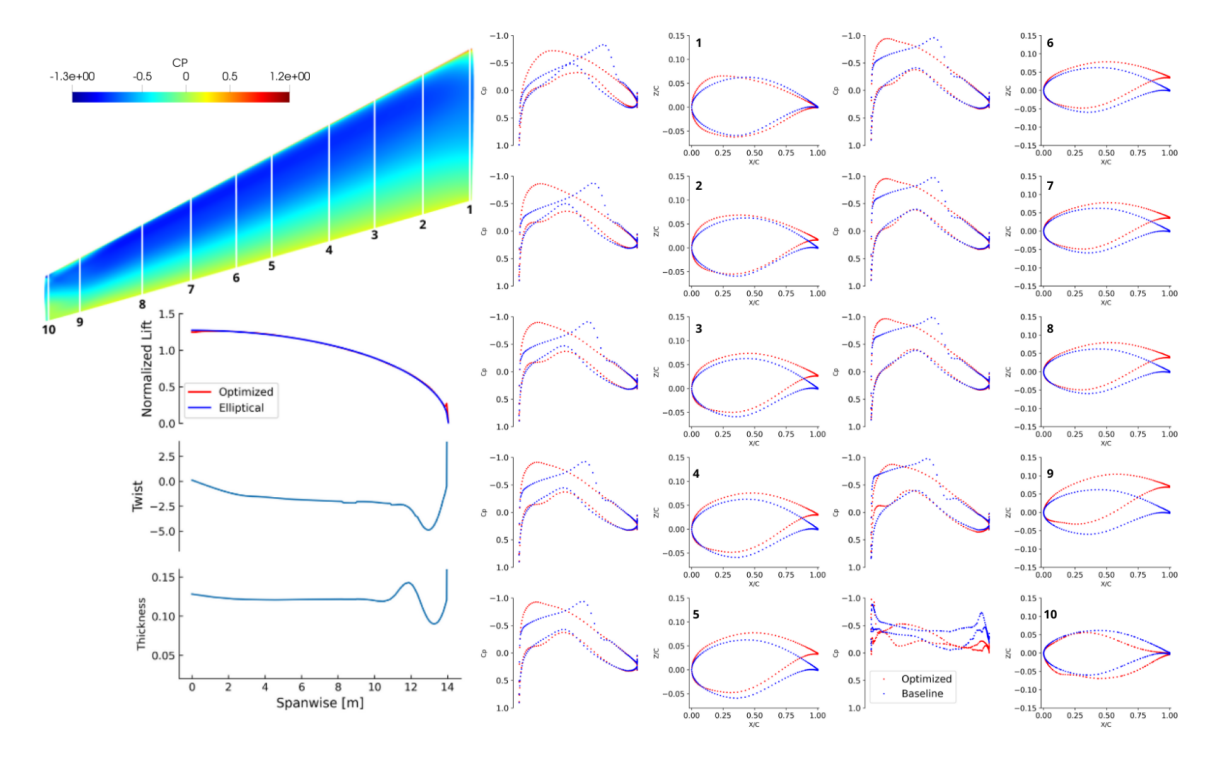
(b) FFD 6-8 results.



(c) FFD 6-14 results.



(d) FFD 6-16 results.



(e) FFD 8-12 results.

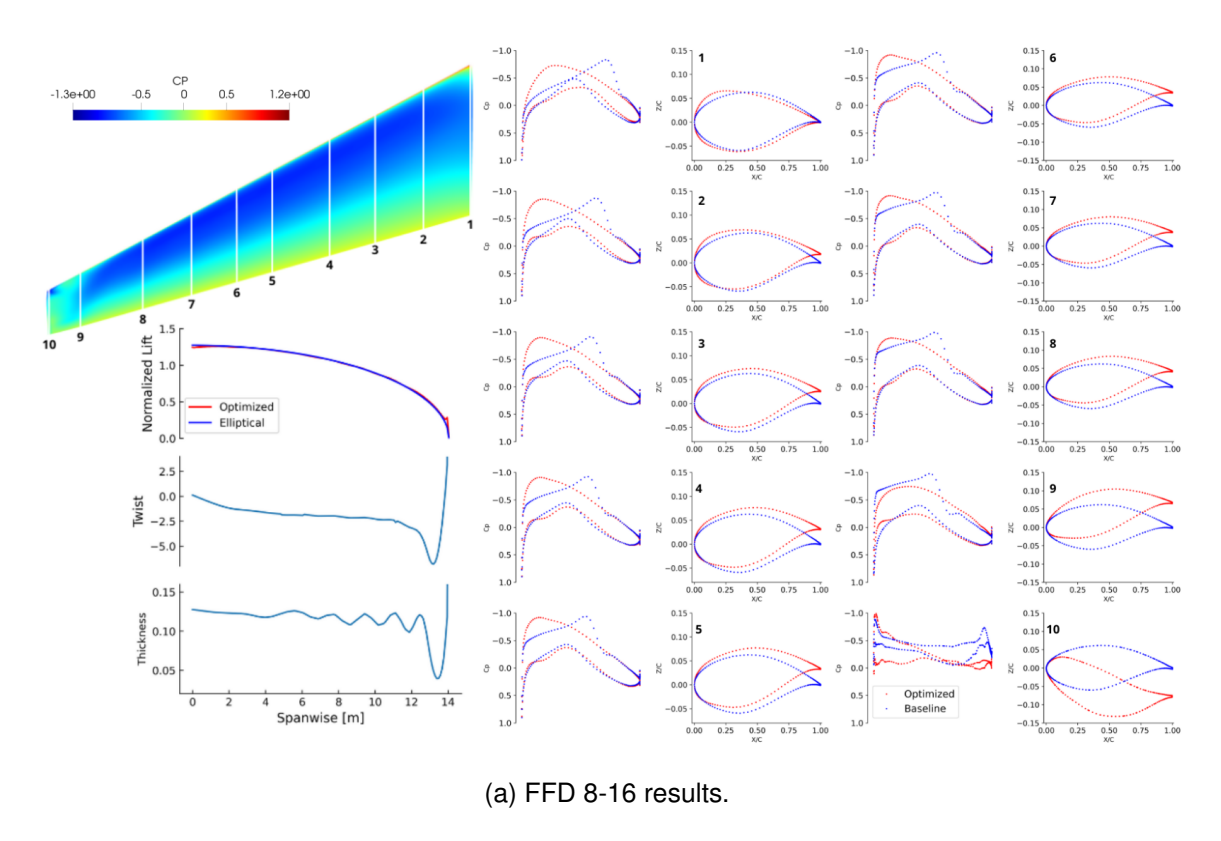
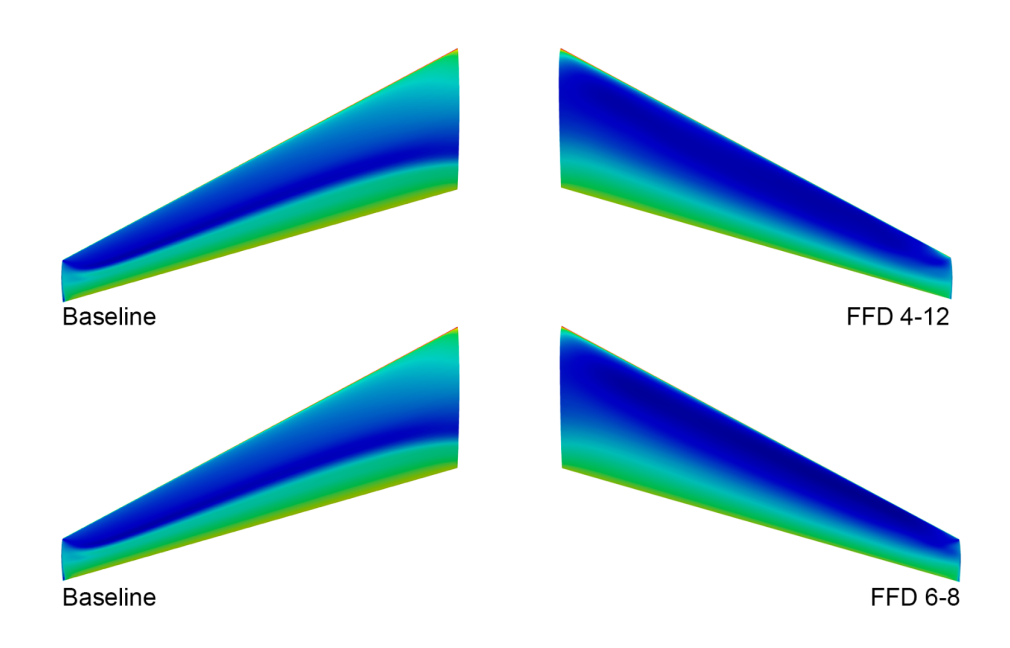


Figure 5 – Optimized designs for varying numbers of FFD control points.

Results in Fig. 6 compare baseline and optimized wing pressure coefficient contours for all of the FFD configurations used here. The baseline configuration presents non-uniform pressure distributions, with prominent regions of high static pressure, which is indicative of shock wave formation on the wing upper surface. The optimized wings demonstrate more uniform pressure distributions, suggesting a successful mitigation of shock waves. Indeed, one can see that, for all FFDs used here, the optimizer leads to shock-free optimal wings. This is a typical result of single-point aerodynamic shape optimization of transonic airfoils and wings. Furthermore, the optimized wings exhibit smoother pressure gradient transitions, contributing to enhanced aerodynamic performance.



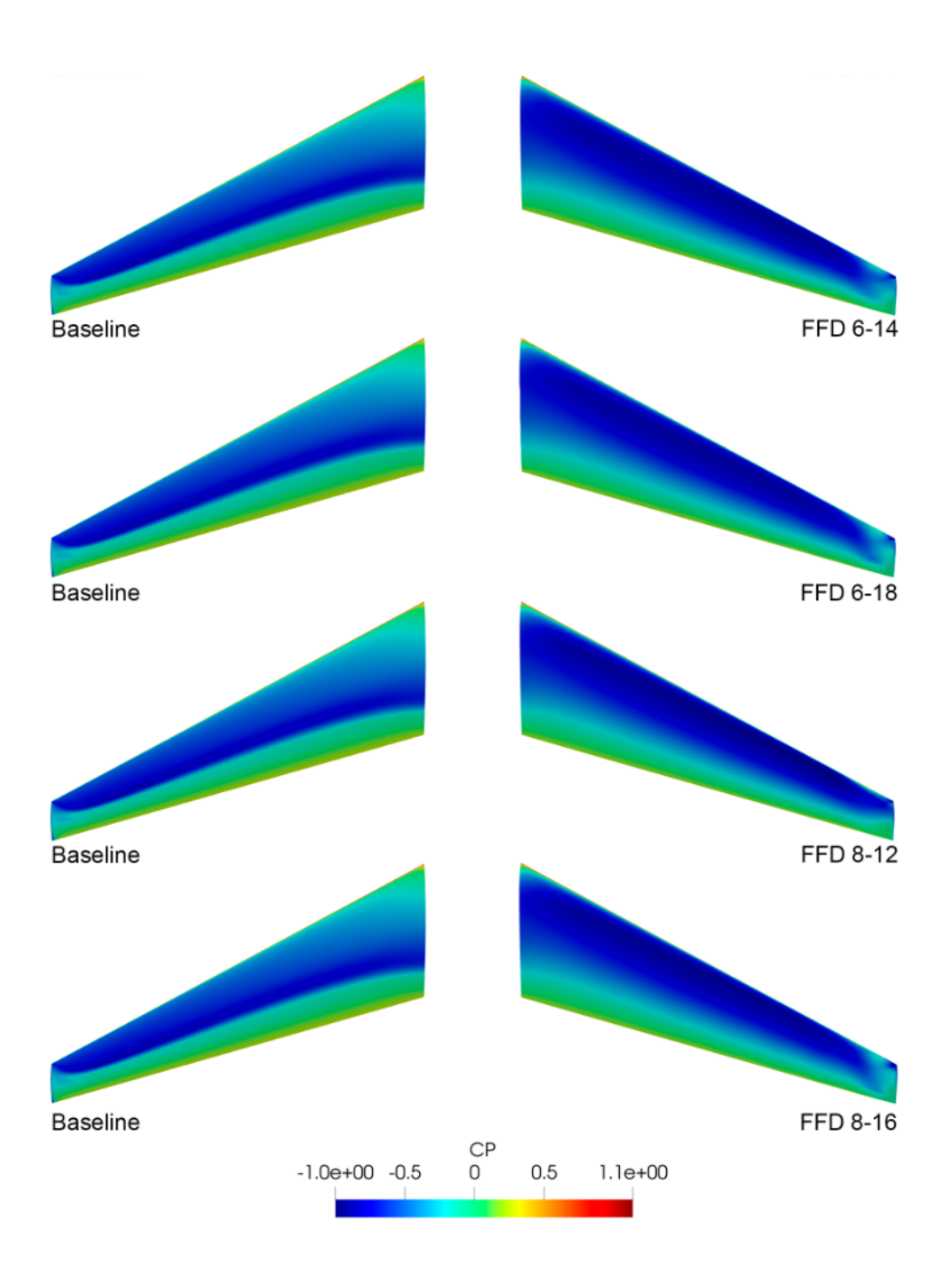
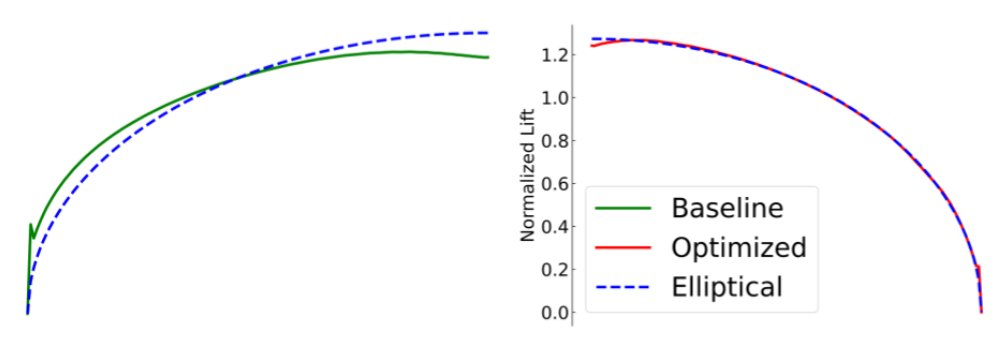
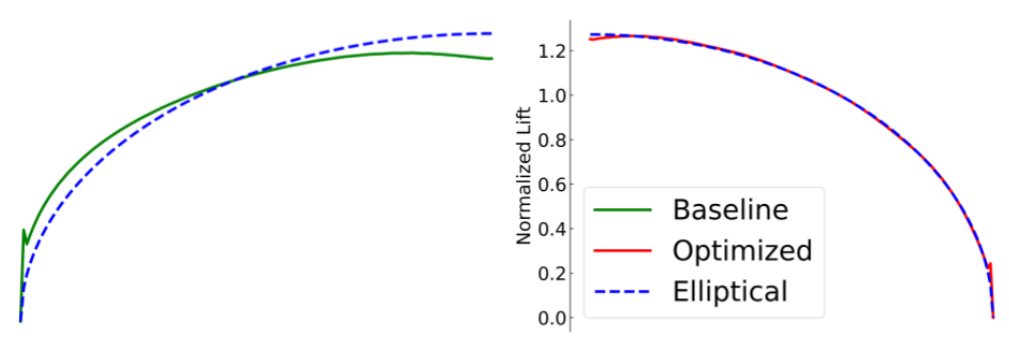


Figure 6 – Pressure coefficient contours for baseline and optimized wings for varying numbers of FFD control points.

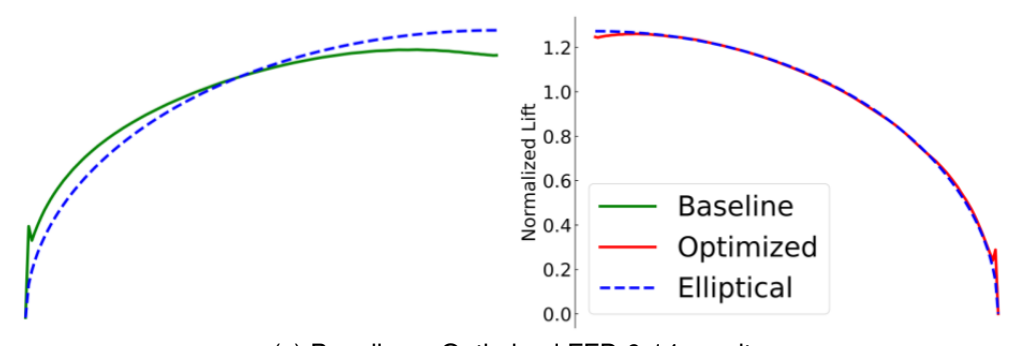
As previously mentioned, the optimized wings exhibit more pronounced twist at the tips, a result of the optimizer's attempt to reduce induced drag and enhance aerodynamic efficiency. Figure 7 illustrates the normalized lift distributions for baseline and optimized wings. As one can see, for all the FFD configurations, the optimized wing normalized lift distributions approach the elliptical one.



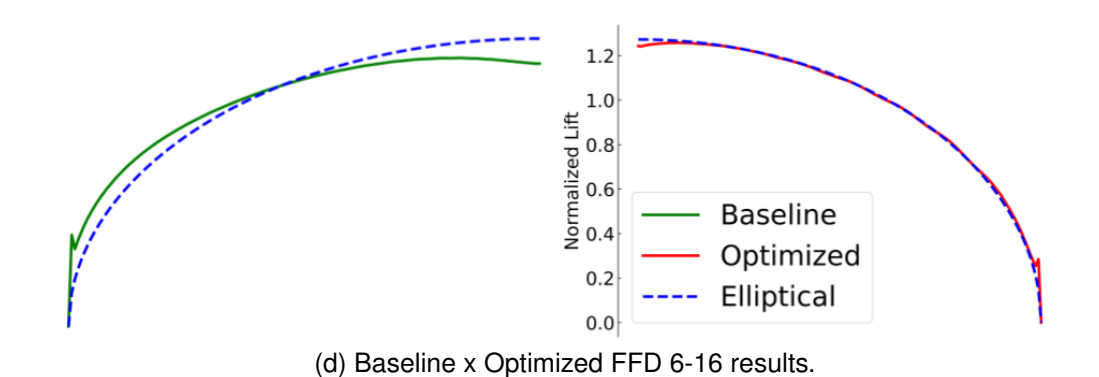
(a) Baseline x Optimized FFD 4-12 results.

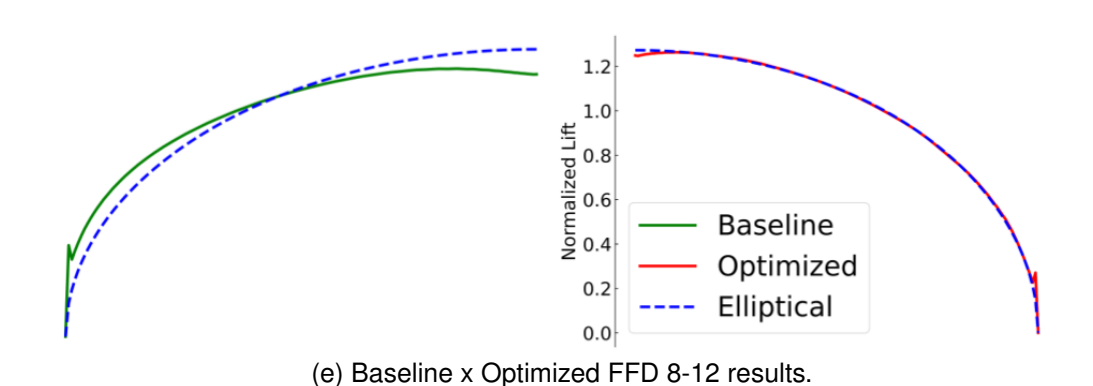


(b) Baseline x Optimized FFD 6-8 results.



(c) Baseline x Optimized FFD 6-14 results.





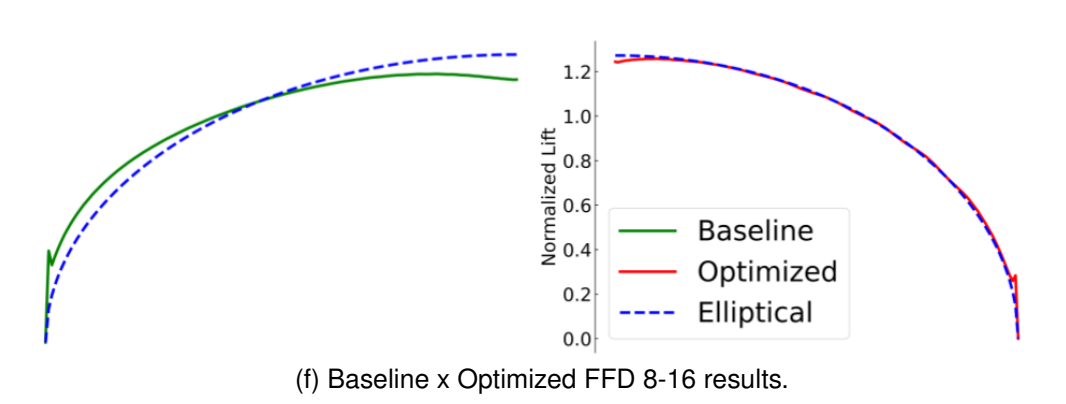


Figure 7 – Normalized lift distribution for baseline and optimized wings for varying numbers of FFD control points.

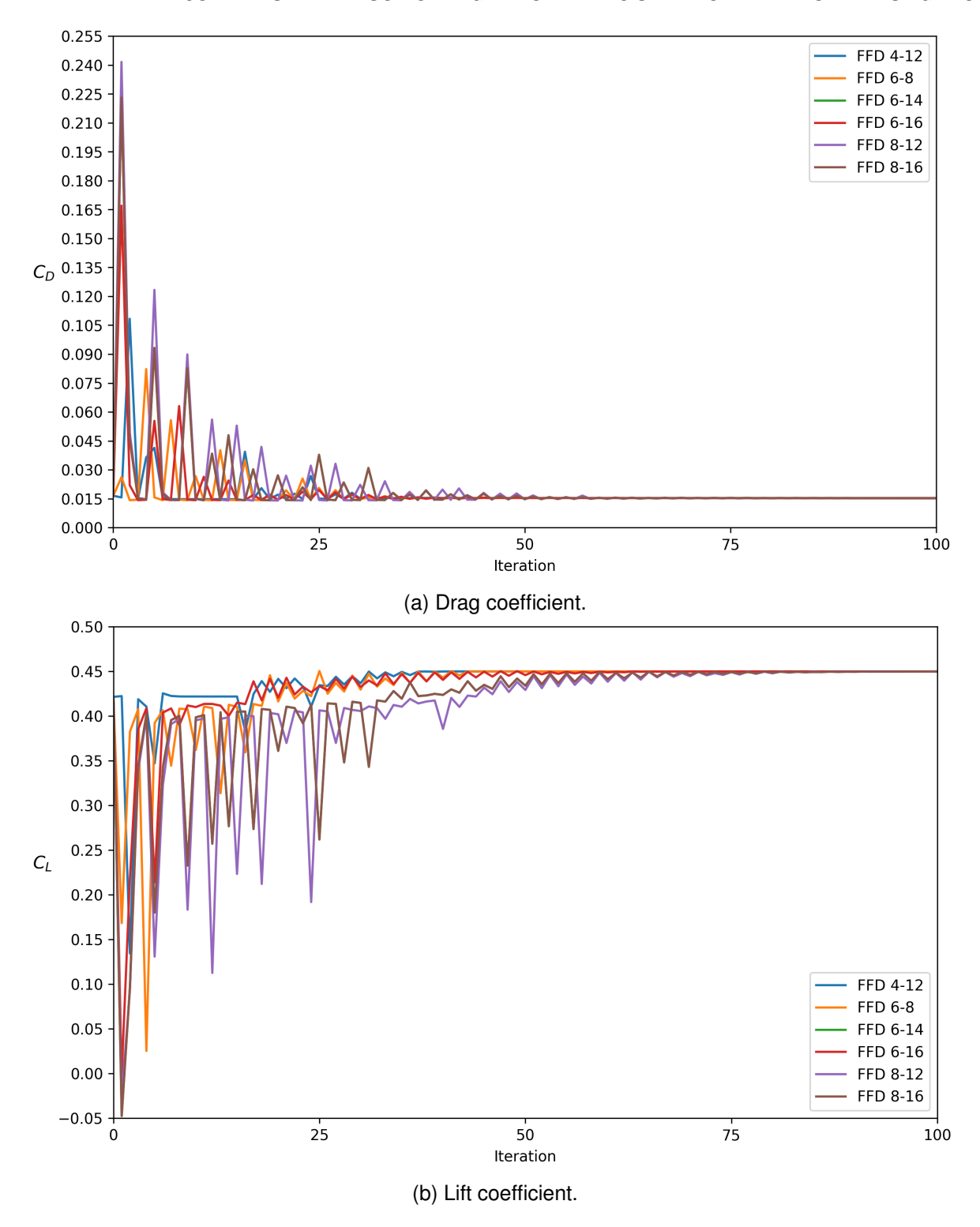


Figure 8 – Lift and drag coefficient convergences throughout the optimization cycles for varying numbers of FFD control points.

Figure 8 depicts the lift and drag coefficient convergences through the optimization cycles for different FFD configurations. Lift and drag coefficient convergence is achieved within the specified tolerances of 1×10^{-6} for our FFD configurations. Lift coefficient oscillations are observed for the FFD 6-14 convergence history, but the optimized wing respects both lift coefficient and geometric constraints.

Our findings highlight the relevance of adjoint-based aerodynamic shape optimization in improving wing aerodynamic efficiency. The single point adjoint-based aerodynamic shape optimization results presented here lead to shock-free transonic wing designs. Transonic wing designs optimized for a single operating point usually present favorable aerodynamic characteristics, but may suffer of

aerodynamic efficiency degradation in off-design conditions. Increasing FFD grid resolution leads to reduced optimized wing drag coefficients, but also results in thickness variations that lead to wavy outer wing designs. This behavior can be fixed by using additional geometric constraints.

5. Conclusions

Transonic wing design is challenging since a number of complex physical phenomena are involved. Some examples are the presence of shock waves, drag divergence, and shock wave-boundary layer interaction. In the context of aerodynamic shape optimization, a complete exploration of these phenomena demands the use of RANS simulations. The associated computational costs, however, make it difficult to address ASO for RANS-based simulations. The adjoint-method consists of a robust and efficient way to compute the required derivatives and, therefore, should be the choice for transonic wing design.

In this paper, we have used the adjoint method to perform transonic lift-constrained wing drag minimization. We use free form deformation grids with varying numbers of control points in both chordwise and spanwise directions. Our single-point ASO simulations lead to shock-free transonic flow, with a trend of drag coefficient reduction with larger FFD grid resolutions. We observe that, in general, more FFD degrees of freedom result in wing shape waviness, specially toward the wing outer sections. This behavior may be corrected by adding more stringent geometric constraints or by exploring additional levels of FFD refinement. The adjoint-base ASO results presented here lead to drag coefficient reductions of up to 16.63% in the operating flight condition, which represents a noticeable aerodynamic efficiency improvement.

6. Acknowledgments

The authors acknowledge the support for the present research provided by Fundação de Amparo à Pesquisa do Estado de São Paulo, FAPESP, under the Research Grant No. 2013/07375-0. Further partial support for the present research was provided by Conselho Nacional de Desenvolvimento Científico e Tecnológico, CNPq, under the Research Grant No. 315411/2023-6. The authors also acknowledge the support provided by Coordenação de Aperfeiçoamento de Pessoal de Nível Superior, CAPES, Brazil, under the Research Grant No. 88887.921353/2023-00.

7. Contact Author Email Address

Lucas Vinicius Rezende Sanches: lucasvrezendesanches@gmail.com

Gustavo Luiz Olichevis Halila: gustavo.halila@embraer.com.br

Felipe Issamu Kitadani Odaguil: felipe.odaguil@embraer.com.br

João Luiz F. Azevedo: joaoluiz.azevedo@gmail.com

8. Copyright Statement

The authors confirm that they, and/or their company or organization, hold copyright on all of the original material included in this paper. The authors also confirm that they have obtained permission, from the copyright holder of any third party material included in this paper, to publish it as part of their paper. The authors confirm that they give permission, or have obtained permission from the copyright holder of this paper, for the publication and distribution of this paper as part of the ICAS proceedings or as individual off-prints from the proceedings.

References

- [1] Vos, R. and Farokhi, S., *Introduction to Transonic Aerodynamics*, Fluid Mechanics and its Applications, Springer, Dordrecht, Netherlands, 2015.
- [2] Bendiksen, O. O., "Review of Unsteady Transonic Aerodynamics: Theory and Applications," *Progress in Aerospace Sciences*, Vol. 47, No. 2, 2011, pp. 135–167.

- [3] Zingg, D. W., Nemec, M., and Pulliam, T. H., "A Comparative Evaluation of Genetic and Gradient-Based Algorithms Applied to Aerodynamic Optimization," *European Journal of Computational Mechanics*, Vol. 17, No. 1–2, January 2008, pp. 103–126.
- [4] Yu, Y., Lyu, Z., Xu, Z., and Martins, J. R. R. A., "On the Influence of Optimization Algorithm and Starting Design on Wing Aerodynamic Shape Optimization," *Aerospace Science and Technology*, Vol. 75, April 2018, pp. 183–199.
- [5] Lyu, Z., Xu, Z., and Martins, J. R. R. A., "Benchmarking Optimization Algorithms for Wing Aerodynamic Design Optimization," Paper No. ICCFD8-2014-0203, *Proceedings of the 8th International Conference on Computational Fluid Dynamics*, Chengdu, Sichuan, China, July 2014.
- [6] Kenway, G. K. W., Mader, C. A., He, P., and Martins, J. R. R. A., "Effective Adjoint Approaches for Computational Fluid Dynamics," *Progress in Aerospace Sciences*, Vol. 110, Article No. 100542, October 2019, pp. 1–26.
- [7] Lions, J. L., *Optimal Control of Systems Governed by Partial Differential Equations*, Springer–Verlag, New York, 1971.
- [8] Bryson, A. E. and Ho, Y.-C., *Applied Optimal Control: Optimization, Estimation, and Control*, John Wiley & Sons, 1975.
- [9] Haug, E. J. and Arora, J. S., "Optimal Mechanical Design Techniques Based on Optimal Control Methods," *Proceedings of the 1st ASME Design Technology Transfer Conference*, New York, NY, October 1974, pp. 65–74.
- [10] Arora, J. S. and Haug, E. J., "Efficient Optimal Design of Structures by Generalized Steepest Descent Programming," *International Journal for Numerical Methods in Engineering*, Vol. 10, 1976, pp. 747–766.
- [11] Pironneau, O., "On Optimum Profiles in Stokes Flow," *Journal of Fluid Mechanics*, Vol. 59, No. 1, 1973, pp. 117–128.
- [12] Pironneau, O., "On Optimum Design in Fluid Mechanics," *Journal of Fluid Mechanics*, Vol. 59, No. 1, 1974, pp. 97–110.
- [13] Jameson, A., "Aerodynamic Design via Control Theory," *Journal of Scientific Computing*, Vol. 3, No. 3, 1988, pp. 233–260.
- [14] Jameson, A., Martinelli, L., and Pierce, N. A., "Optimum Aerodynamic Design Using the Navier–Stokes Equations," *Theoretical and Computational Fluid Dynamics*, Vol. 10, No. 1–4, 1998, pp. 213–237.
- [15] Nielsen, E. J. and Anderson, W. K., "Aerodynamic Design Optimization on Unstructured Meshes Using the Navier–Stokes Equations," *AIAA Journal*, Vol. 37, No. 11, 1999, pp. 1411–1419.
- [16] Buckley, H. P. and Zingg, D. W., "Approach to Aerodynamic Design Through Numerical Optimization," *AIAA Journal*, Vol. 51, No. 8, August 2013, pp. 1972–1981.
- [17] Koo, D. and Zingg, D. W., "Investigation into Aerodynamic Shape Optimization of Planar and Nonplanar Wings," *AIAA Journal*, Vol. 56, No. 1, August 2018, pp. 250–263.
- [18] Chernukhin, O. and Zingg, D. W., "Multimodality and Global Optimization in Aerodynamic Design," *AIAA Journal*, Vol. 51, No. 6, June 2013, pp. 1342–1354.
- [19] Reist, T. A. and Zingg, D. W., "Aerodynamically Optimal Regional Aircraft Concepts: Conventional and Blended-Wing-Body Designs," AIAA Paper No. 2014-0905, *Proceedings of the 52nd Aerospace Sciences Meeting*, National Harbor, MD, January 2014.
- [20] Lyu, Z., Kenway, G. K. W., and Martins, J. R. A., "Aerodynamic Shape Optimization Investigations of the Common Research Model Wing Benchmark," *AIAA Journal*, Vol. 53, No. 4, April 2015, pp. 968–985.
- [21] Chen, S., Lyu, Z., Kenway, G. K. W., and Martins, J. R. R. A., "Aerodynamic Shape Optimization of the Common Research Model Wing-Body-Tail Configuration," *Journal of Aircraft*, Vol. 53, No. 1, January 2016, pp. 276–293.
- [22] Kenway, G. K. W. and Martins, J. R. R. A., "Multi-point High-fidelity Aerostructural Optimization of a Transport Aircraft Configuration," *Journal of Aircraft*, Vol. 51, No. 1, Jan-Feb 2014, pp. 144–160.
- [23] Gray, J. S. and Martins, J. R. A., "Coupled Aeropropulsive Design Optimization of a Boundary Layer Ingestion Propulsor," *The Aeronautical Journal*, 2018, pp. 1–19.
- [24] Kroo, I. and Sturdza, P., "Laminar Flow Control A Systems Approach," AIAA Paper No. 2003-774, *Proceedings of the 41st Aerospace Sciences Meeting and Exhibit*, AIAA, Reno, NV, January 2003.
- [25] Sturdza, P., "Extensive Supersonic Natural Laminar Flow on the Aerion Business Jet," AIAA Paper No. 2007-0685, Proceedings of the 45th AIAA Aerospace Sciences Meeting and Exhibit, Reno, NV, January 2007, AIAA 2007–0685.
- [26] Driver, J. and Zingg, D. W., "Numerical Aerodynamic Optimization Incorporating Laminar-Turbulent Transition Prediction," *AIAA Journal*, Vol. 45, No. 8, 2007, pp. 1810–1818.
- [27] Halila, G. L. O., Martins, J. R. R. A., and Fidkowski, K. J., "Adjoint-Based Aerodynamic Shape Optimiza-

- tion Including Transition to Turbulence Effects," *Aerospace Science and Technology*, Vol. 107, Article No. 106243, December 2020, pp. 1–15.
- [28] Mavriplis, D., Yang, Z., and Anderson, E. M., "Adjoint Based Optimization of a Slotted Natural Laminar Flow Wing for Ultra Efficient Flight," AIAA Paper No. 2020-1292, *Proceedings of the AIAA Scitech 2020 Forum*, Orlando, FL, January 2020.
- [29] Rumpfkeil, M. and Zingg, D., "The Optimal Control of Unsteady Flows with a Discrete Adjoint Method," *Optimization and Engineering*, Vol. 11, 2010, pp. 5–22.
- [30] Jameson, A. J., Schmidt, W., and Turkel, E., "Numerical Solution of the Euler Equations by a Finite-Volume Method Using Runge-Kutta Time-Stepping Schemes," AIAA Paper No. 1981-1259, 14th AIAA Fluid and Plasma Dynamics Conference, Palo Alto, CA, June 1981.
- [31] Turkel, E. and Vatsa, V. N., "Effects of Artificial Viscosity on Three-Dimensional Flow Solutions," *AIAA Journal*, Vol. 32, 1994, pp. 39–45.
- [32] van Leer, B., "Towards the Ultimate Conservative Difference Scheme. V. A Second-Order Sequel to Godunov's Method," *Journal of Computational Physics*, Vol. 32, 1979, pp. 101–136.
- [33] Roe, P. L., "Approximate Riemann Solvers, Parameter Vectors, and Difference Schemes," *Journal of Computational Physics*, Vol. 43, 1981, pp. 357–372.
- [34] Klopfer, G., Hung, C., Van der Wijngaart, R., and Onufer, J., "A Diagonalized Diagonal Dominant Alternating Direction Implicit (D3ADI) Scheme and Subiteration Correction," AIAA Paper No. 1998-2824, 29th AIAA Fluid Dynamics Conference, Albuquerque, NM, June 1998.
- [35] Yildirim, A., Kenway, G. K. W., Mader, C. A., and Martins, J. R. A., "A Jacobian-Free Approximate Newton–Krylov Startup Strategy for RANS Simulations," *Journal of Computational Physics*, Vol. 397, Article No. 108741, November 2019, pp. 1–34.
- [36] Nemec, M. and Zingg, D. W., "Newton–Krylov Algorithm for Aerodynamic Design Using the Navier–Stokes Equations," *AIAA Journal*, Vol. 40, No. 6, June 2002, pp. 1146–1154.
- [37] Mader, C. A., Kenway, G. K. W., Yildirim, A., and Martins, J. R. R. A., "ADflow: An Open-Source Computational Fluid Dynamics Solver for Aerodynamic and Multidisciplinary Optimization," *Journal of Aerospace Information Systems*, Vol. 17, No. 9, September 2020, pp. 508–527.
- [38] Kenway, G. K., Kennedy, G. J., and Martins, J. R. A., "A CAD-Free Approach to High-Fidelity Aerostructural Optimization," AIAA Paper No. 2010-9231, *Proceedings of the 13th AIAA/ISSMO Multidisciplinary Analysis Optimization Conference*, Fort Worth, TX, September 2010.
- [39] Secco, N., Kenway, G. K. W., He, P., Mader, C. A., and Martins, J. R. R. A., "Efficient Mesh Generation and Deformation for Aerodynamic Shape Optimization," *AIAA Journal*, Vol. 59, No. 4, April 2021, pp. 1151– 1168.
- [40] Sederberg, T. W. and Parry, S. R., "Free-form Deformation of Solid Geometric Models," *SIGGRAPH Comput. Graph.*, Vol. 20, No. 4, Aug. 1986, pp. 151–160.
- [41] Luke, E., Collins, E., and Blades, E., "A Fast Mesh Deformation Method Using Explicit Interpolation," *Journal of Computational Physics*, Vol. 231, No. 2, Jan. 2012, pp. 586–601.
- [42] Nielsen, E. J. and Park, M. A., "Using an Adjoint Approach to Eliminate Mesh Sensitivities in Computational Design," *AIAA Journal*, Vol. 44, No. 5, 2006, pp. 948–953.
- [43] Widhalm, M., Brezillon, J., Ilic, C., and Leicht, T., "Investigation on Adjoint Based Gradient Computations for Realistic 3D Aero-Optimization," AIAA Paper No. 2010-9129, 13th AIAA/ISSMO Multidisciplinary Analysis and Optimization Conference, No. September, Fort Worth, TX, 2010, pp. 1–17.
- [44] Spalart, P. R. and Allmaras, S. R., "A One-Equation Turbulence Model for Aerodynamic Flows," AIAA Paper No. 92-0439, *Proceedings of the 30th AIAA Aerospace Sciences Meeting and Exhibit*, Reno, NV, Jan. 1992.
- [45] Goncalves, E. and Houdeville, R., "Turbulence Model and Numerical Scheme Assessment for Buffet Computations," *International Journal for Numerical Methods in Fluids*, Vol. 46, No. 11, December 2004, pp. 1127–1152.
- [46] Menter, F. R., "Two-Equation Eddy Viscosity Turbulence Models for Engineering Applications," *AIAA Journal*, Vol. 32, No. 8, August 1994, pp. 1598–1605.
- [47] Allmaras, S. R. and Johnson, F. T., "Modifications and Clarifications for the Implementation of the Spalart-Allmaras Turbulence Model," *Seventh International Conference on Computational Fluid Dynamics (IC-CFD7)*, 2012, pp. 1–11.
- [48] Martins, J. R. A. and Ning, A., Engineering Design Optimization, Cambridge University Press, 2022.
- [49] Nadarajh, S. and Jameson, A., "A Comparison of the Continuous and Discrete Adjoint Approach to Automatic Aerodynamic Optimization," AIAA Paper No. 2000-0667, *Proceedings of the 38th AIAA Aerospace Sciences Meeting and Exhibit*, Reno, NV., Jan. 2000.

- [50] Peter, J. E. V. and Dwight, R. P., "Numerical Sensitivity Analysis for Aerodynamic Optimization: A Survey of Approaches," *Computers and Fluids*, Vol. 39, No. 3, March 2010, pp. 373–391.
- [51] Giles, M. B. and Pierce, N. A., "An Introduction to the Adjoint Approach to Design," *Flow, Turbulence and Combustion*, Vol. 65, 2000, pp. 393–415.
- [52] Griewank, A., Evaluating Derivatives, SIAM, Philadelphia, 2000.
- [53] Kraft, D., "Algorithm 733: TOMP–Fortran Modules for Optimal Control Calculations," *ACM Transactions on Mathematical Software*, Vol. 20, No. 3, September 1994, pp. 262–281.
- [54] Nocedal, J. and Wright, S. J., Numerical Optimization, Springer-Verlag, 2nd ed., 2006.
- [55] "MACH-Aero Tutorial. MDO Laboratory, University of Michigan." https://mdolab-mach-aero.readthedocs-hosted.com/en/latest/machAeroTutorials/intro.html.